David O. Smallwood
Sandia National Laboratories
Albuquerque, NM 87185

Characterization and Simulation of Transient Vibrations Using Band Limited Temporal Moments

A method is described to characterize shocks (transient time histories) in terms of the Fourier energy spectrum and the temporal moments of the shock passed through a contiguous set of band pass filters. The product model is then used to generate of a random process as simulations that in the mean will have the same energy and moments as the characterization of the transient event. © *1994 John Wiley & Sons, Inc.*

INTRODUCTION

The methods used for characterizing transient vibrations or shocks usually involve one of two methods, specification of the time history or specification of the shock response spectrum. Less commonly used are the Fourier energy spectrum (Baca, 1989), the method of least favorable response (Shinozuka, 1970; Smallwood, 1973), nonstationary models (Mark, 1972; Himelblau and Piersol, 1989), and most recently wavelets (Chui, 1992). In this article a new method is described based on temporal moments and the Fourier energy spectrum.

Specification of Time History

The specification of the time history (for example, a 100 ms, 10 × g peak, haversine) usually assumes the time history is relatively simple and deterministic. A very common practice is to define the shock in terms of a waveform that can be produced on a variety of shock machines like drop tables. A very common waveform is a haversine which can be completely described in terms of its amplitude and duration. Specifications are carefully written to describe how closely a test time history must conform to the ideal waveform.

In practice shocks are often complex and somewhat random in character. The shocks are double sided (have both positive and negative peaks) and are not easily characterized in terms of a simple waveform.

Shock Response Spectrum (SRS) Method

SRS was developed to reduce the complexity mentioned above to a simple measure, that is, the response of a single-degree-of-freedom (SDOF) system to the shock. The SRS is the peak response of a SDOF system to a transient input, as a function of the natural frequency of the SDOF system. A great variety of methods were devel-

Received February 17, 1994; Accepted April 25, 1994.
Shock and Vibration, Vol. 1, No. 6, pp. 507–527 (1994)

CCC 1070-9622/94/060507-21

oped to produce time histories with a specified SRS that could be used as test waveforms to qualify equipment to a shock environment described using the SRS (Smallwood, 1975, 1986).

These time histories that matched a specified SRS could then be reproduced on shakers or other equipment. Classical waveforms on conventional shock machines are also used. Only recently the SRS method, instead of tolerances on the time history, has been used to define the requirements. The usual method is to require the SRS of the test to overlay the SRS of the requirement within some tolerance.

The SRS is the method most commonly used today to characterize shocks, and to specify shock environments. However, the shock spectrum has its own set of limitations and is subject to misuse if these limitations are not well understood or are ignored. One of the most serious limitations of the SRS is that it says nothing about the duration of the event. To prevent misuse of the SRS specification (as for example, meeting an SRS specification with a long sine sweep test, which has been done) limitations on the duration of the test input are often imposed. Another abuse arises because the environment is often an oscillatory waveform and the test simulates the environment with a simple nonoscillatory waveform. The test waveform often has a higher peak amplitude, a shorter duration, and a much larger velocity change than the actual environment, which can led to serious overtests and undertests. Again the SRS contains little information about the oscillatory nature of the waveform.

If the SRS is accurately calculated over a wide range of natural frequencies, the following information can be deduced. The velocity change is contained in the low frequency end of the SRS. The peak level of the shock is equal to the SRS at very high frequencies. A large ratio of the peak level in the SRS to the value of the SRS at very high frequencies indicates an oscillatory waveform. Unfortunately, the SRS is often not specified over a wide enough frequency range. The SRS often is inaccurate at low frequencies, and the test specification is often an envelope of an ensemble of environments further obscuring the underlying SRS.

Another abuse is to assume the SRS measures the spectral content of a shock. The SRS does tend to peak where the spectral content of the shock is higher, but an SDOF system can respond where the spectral content is very low. An example is at very high frequencies where the SRS equals the peak value of the shock although the spectral content of the shock can be very low. Further simplifications and assumptions must be used when applying the SRS to multiple DOF systems. It should also be recognized that the SRS does not directly characterize the shock, but rather characterizes the response of an SDOF system to the shock. Neither a time history specification nor the shock spectrum specification lend themselves well to a statistical treatment of the uncertainties in the shock. Baca (1989), Hart and Hasselman (1976), and others have looked at different measures of shock environments to overcome some of the limitations of the above methods.

Fourier Energy Spectrum

The Fourier spectrum offers an attractive alternative to SRS. The theory is rich with many applications of the Fourier spectrum. The Fourier spectrum is easy to compute using modern FFT (fast Fourier transform) methods. The Fourier spectrum does measure the spectral content of the waveform, but a serious limitation of the Fourier Spectrum is the fact that it is complex. The magnitude has intuitive meaning, but the phase information is harder to present and interpret. Some authors have proposed using only the amplitude information and picking the phase to maximize the response.

Least Favorable Response

One method of specifying the phase is the method of least favorable response (Hart and Hasselman, 1976; Shinozuka, 1970; Smallwood, 1973). The idea is to pick the phase of the Fourier spectrum, given the envelope of the Fourier energy spectrum, to maximize the response of the system under test. This is the least favorable input, from the viewpoint of system survival. This method has not gained wide acceptance for at least two reasons. One is the problem of determining where on the structure to maximize the response, and the other is the perceived over conservatism of the test.

Nonstationary Models

Vibration environments have long been characterized with random vibration using stationary models. The principal tool for this description is

the auto (power) spectral density. We commonly run vibration tests controlling a specific power spectrum. We have only recently begun to seriously consider modeling and subsequent testing of nonstationary events (Hart and Hasselman, 1976; Paez and Baca, 1988; Merritt, 1993; Himelblau and Piersol, 1989). The most common model for these environments is to assume a stationary underlying process multiplied by a deterministic time varying modulating function (the product model discussed below). Sometimes the underlying stationary spectrum is allowed to vary slowly with time. These methods lead naturally to a stationary description as the record times become long.

Wavelets

A recent development has been to describe nonstationary waveforms in terms of wavelets (Chui, 1992). This technique is most commonly applied to long records with a highly nonstationary characteristic, like speech. The technique has been used to study the impulse response of systems, but the author is not aware of this technique being extended to single transients with a large random component. This could be a subject of future research, but is not addressed here. The attempt in this article is to characterize the transient with as few parameters as possible. Because the wavelet transform is invertible, it contains all the information in the original waveform. The wavelet transform does not attempt to summarize the characteristics of a transient in a few parameters. The wavelet transform does give a 3-dimensional view of the transient in amplitude, time, and frequency.

Method Based on Fourier Energy and Band-Limited Temporal Moments

The proposed method addresses those environments where the time durations are too short for even the nonstationary models mentioned above to be meaningful, but with a large random contribution that makes the method of time history specification or SRS specification less desirable. The nonstationary models require durations long enough or ensembles to make statistically significant statements about the underlying spectrum and the modulating envelope. The shock models should be based on methods that can lead to statistically meaningful statements.

The method will use the magnitude of the Fourier spectrum, more specifically the magnitude squared or energy spectrum, to describe the spectral content of the shock. The spectrum is smoothed or formed from an ensemble average to generate statistically significant values. The method will use temporal moments of the time histories to describe how the energy is distributed in time. It is shown that the distribution of the energy in time is related to the phase of the Fourier spectrum.

Before proceeding with a description of the method, it is necessary to define the temporal moments, give an interpretation of the first few moments, and describe a few of the properties of the moments.

TEMPORAL MOMENTS OF A TIME HISTORY

The moments are analogous to the moments of probability density functions. The square of the time history is used for several reasons. The problem of negative amplitudes is avoided. By using the squared time history there are useful properties, relating time and frequency, between the temporal moments and moments in the frequency domain.

The ith temporal moment, $m_i(a)$, of a time history, $x(t)$, about a time location, a, will be defined as

$$m_i(a) = \int_{-\infty}^{\infty} (t - a)^i \, x^2(t) dt. \tag{1}$$

The moments prove to be very useful to describe simple time history shapes and to describe the envelopes of more complicated shock time histories.

Two special cases are defined. First, if the time shift, a, is 0 the argument will be dropped for simplicity

$$m_i = m_i(0). \tag{2}$$

Second, the central moments are defined about a value, τ, that produces a zero first moment, that is,

$$m_1(\tau) = 0. \tag{3}$$

Solving Eq. (1) for $a = \tau$ gives,

$$\tau = m_1/m_0. \tag{4}$$

The first five moments (0–4) about τ are of special interest and will be given special names.

The zero order moment is independent of the shift, a, and the centroid, τ,

$$m_0(a) = m_0 = E. \tag{5}$$

This value is the integral of the magnitude squared of the time history and is called the time history energy. Assume the energy is finite. The energy in the time domain is related to the energy in the frequency domain through the Fourier transform. Let $X(\omega)$ be the Fourier transform of $x(t)$. Then Parseval's formula (Papoulis, 1962) gives,

$$\int_{-\infty}^{\infty} |x(t)|^2 \, dt = \frac{1}{2\pi} \int_{-\infty}^{\infty} |X(\omega)|^2 \, d\omega. \tag{6}$$

The magnitude squared of the Fourier spectrum, $|X(\omega)|^2 = \Phi(\omega)$, is called the energy spectrum. The square root of the energy normalized by the rms duration (to be defined later) will be called the root energy amplitude, REA or, A_e, and will provide a convenient way to describe the energy,

$$A_e = \sqrt{E/D}. \tag{7}$$

The root energy amplitude will conveniently have the same units as $x(t)$.

As discussed earlier, the first moment normalized by the energy gives the time where the centroid of the energy is located, Eq. (4), and is called the central time or centroid, τ. Because the origin of the time axis is often arbitrary, the central time is often important only in a relative sense. The higher moments are also calculated around the centroid for convenience, and to make the parameters independent of the time origin.

The second central moment normalized by the energy is defined as the mean square duration, D^2, of the time history,

$$D^2 = m_2(\tau)/\mathrm{E}. \tag{8}$$

The rms duration, D, is useful to describe the duration of complex waveforms where more conventional definitions of duration are difficult to apply. As with probability distributions we expect most of the significant part of the transient to be within plus or minus a few rms durations of the centroid.

The third central moment normalized by the energy is defined as the skewness, S_t. The t subscript is used to indicate this quantity has units of time.

$$S_t^3 = m_3(\tau)/E. \tag{9}$$

A nondimensional measure of skewness, S, normalized by the rms duration is also useful.

$$S = S_t/D. \tag{10}$$

Skewness is a parameter that describes the shape of the function. A positive skewness indicates a time history that has high amplitudes on the left of the centroid and a long low-amplitude tail on the right of the centroid. A negative skewness indicates a long low-amplitude tail on the left and high amplitudes on the right of the centroid. Waveforms that are symmetrical about the centroid have zero skewness. If a waveform envelope is unimodal (having only one peak) higher moments than skewness usually add little information. Note that if a family of shapes all have positive skewness, a family of shapes can easily be generated with negative skewness by simply reversing the time histories of the first family.

The importance of matching the skewness in a shock test is not clear. In a qualitative sense, the rate of increase of the input will influence the peak response. This was demonstrated in the least favorable responses work (Smallwood, 1973). Matching the central times and rms durations is clearly more important. As will be seen later, matching the skewness improves the appearance of the waveforms. A large skewness indicates a short rise or fall time which can effect the response of a system. Quantitatively the effect on system response is not clear.

The fourth central moment normalized by the energy, K_t, is called kurtosis

$$K_t^4 = m_4(\tau)/E. \tag{11}$$

A normalized kurtosis can be defined as

$$K = K_t/D. \tag{12}$$

The kurtosis may be useful for time histories whose envelopes are not unimodal, that is, have more than one maximum, and as a descriptor of where the peaks in the envelope of the time history occur.

High moments can similarly be defined, but

are not necessary for this article. The intent is to describe the waveform with as few parameters as possible. Relationships between the various moments can be easily derived and are stated below.

First, the basic moments about time zero are given in terms of the normalized central moments.

$$m_0 = E \tag{13}$$

$$m_1 = E\tau \tag{14}$$

$$m_2 = E(D^2 + \tau^2) \tag{15}$$

$$m_3 = E(S^3 + 3\tau D^2 + \tau^3) \tag{16}$$

$$m_4 = E(K_t^4 + 4S_t^3\tau + 6D^2\tau^2 + \tau^4). \tag{17}$$

Second, the normalized central moments are given in terms of the basic moments about zero time.

$$E = m_0 \tag{18}$$

$$\tau = m_1/m_0 \tag{19}$$

$$D^2 = (m_2/m_0) - (m_1/m_0)^2 \tag{20}$$

$$S_t^3 = (m_3/m_0) - 3(m_2m_1/m_0^2) + 2(m_1/m_0)^3 \tag{21}$$

$$K_t^4 = (m_4/m_0) - 4(m_3m_1/m_0^2) + 6(m_2m_1^2/m_0^3) - 3(m_1/m_0)^4. \tag{22}$$

Third, the basic moments about a time, a, are given in terms of the normalized central moments.

$$m_0(a) = m_0 = E \tag{23}$$

$$m_1(a) = m_1 - am_0 = E(\tau - a) \tag{24}$$

$$m_2(a) = m_2 - 2am_1 + a^2m_0 = E(D^2 + (\tau - a)^2) \tag{25}$$

$$m_3(a) = m_3 - 3am_2 + 3a^2m_1 - a^3m_0 = E(S_t^3 + 3\tau D^2 + \tau^3 - 3aD^2 - 3a\tau^2 + 3a^2\tau - a^3). \tag{26}$$

From Eq. (25), it is clear that $m_2(a)$ is a minimum when $a = \tau$. This is the reason the rms duration, D, is defined by the second moment about τ.

Some Properties of Temporal Moments

RMS Duration and Ripple in Frequency Domain. The following identity relates the rms duration of a time history with unity energy to the ripple (variations in the first derivative of amplitude and phase) of the Fourier spectrum (Papoulis, 1962).

$$\int_{-\infty}^{\infty} t^2|x(t)|^2\,dt = \frac{1}{2\pi} = \int_{-\infty}^{\infty}\left[\left|\frac{dA}{d\omega}\right|^2 + A^2\left|\frac{d\phi}{d\omega}\right|^2\right]d\omega \tag{27}$$

where

$$X(\omega) = A(\omega)e^{i\phi(\omega)} \tag{28}$$

From Eq. (27), we conclude that high ripple in the magnitude, A, or in the phase angle, ϕ, results in time histories with long durations. If the amplitude is fixed, the ripple in the phase directly controls the duration of the time history. As the phase becomes smooth the rms time duration decreases.

Uncertainty Principle. To simplify the development assume that the energy is unity and the central moments are used. The duration in time is then given by

$$D^2 = m_2. \tag{29}$$

Let $x(t)$ and $X(\omega)$ be Fourier transform pairs. Define the mean square duration in frequency as,

$$D_\omega^2 = \int_{-\infty}^{\infty} \omega^2|X(\omega)|^2\,d\omega. \tag{30}$$

The uncertainty principle (Papoulis, 1962) states that, if $x(t)$ vanishes at infinity faster than $1/\sqrt{t}$ then

$$DD_\omega \geq \sqrt{\pi/2}. \tag{31}$$

The equality holds for only one family of time histories, Gaussian time histories, of the form

$$x(t) = \sqrt{\alpha/\pi}\; e^{-\alpha t^2}. \tag{32}$$

The uncertainty principle states that we cannot have a signal that is both band limited and time limited. It also indicates that as we narrow the bandwidth of a signal, the duration will necessarily increase.

For example, consider a band limited signal

with a flat spectrum from 0 to f_0, and an rms duration of 0.5 ms. This duration is chosen because it is the approximate duration of a waveform used in a later example. Equations (30) and (31) indicate this waveform can have a minimum cutoff frequency, f_0, of 276 Hz. If a broad band waveform with an arms duration of 0.5 ms is filtered with a low pass filter, the rms duration of the filtered waveform will be significantly lengthened if the cutoff frequency approaches this limit. The bandwidth chosen for a later example is 2500 Hz, almost 10 times this limit. Later it is proposed that a shock time history be filtered with a set of bandpass filters and the time moments of the filtered signals estimated. The uncertainty principal will limit how narrow these filters can be. The bandwidth should be much larger than the limits imposed by the uncertainty theorem to avoid the time dilation caused by the filter. As the time duration of the waveform increases, the filters can become more narrow. As the filters narrow, the energy in the filtered signal can be normalized to provide a power spectrum estimate.

For transients with a large random content we will see later that the variance of the estimates will also limit the bandwidth of the filters.

Adding Moments. Let

$$z(t) = x(t) + y(t). \tag{33}$$

It can be easily shown that the jth moment of $z(t)$ about a, ${}_zm_j(a)$, is given by

$$\begin{aligned} {}_zm_j(a) &= {}_xm_j(a) + {}_ym_j(a) \\ &\quad + 2\int_{-\infty}^{\infty} (t-a)^j x(t)y(t)\,dt. \end{aligned} \tag{34}$$

Moments can be added for the special case where the integral in Eq. (34) is 0. The integral will be 0 if $x(t)$ and $y(t)$ are random, uncorrelated, and 0 mean. In this case,

$${}_zm_j(a) = {}_zm_j(a) + {}_xm_j(a). \tag{35}$$

If the integral in Eq. (34) is 0 or small relations between the energy, time to the centroid, and rms duration can be given,

$$E_z = E_x + E_y \tag{36}$$

$$\tau_z = \frac{E_x\tau_x + E_y\tau_y}{E_x + E_y} \tag{37}$$

$$D_z^2 = \frac{E_x(D_x^2 + \tau_x^2) + E_y(D_y^2 + \tau_y^2)}{E_x + E_y} - \frac{(E_x\tau_x + E_y\tau_y)^2}{(E_x + E_y)^2}. \tag{38}$$

Equations for the higher moments get more complicated. Thus, adding central moments for even the simple case of uncorrelated x and y gets complicated. It is probably better to use Eq. (35), and then compute the central moments from Eqs. (18)–(22).

Time Reversals. Let

$$g(t) = f(-t). \tag{39}$$

It can be shown that the jth moment of $g(t)$, is related to the jth moment of $f(t)$ by

$${}_gm_j = (-1)^j{}_fm_j. \tag{40}$$

Thus we see that the even moments are the same, and the odd moments differ only in sign. The properties of several common waveforms are given in Appendix A.

Product Model

A commonly used model for nonstationary random data, which will be used extensively in the simulation section, is the product model. Consider a stationary random signal with a fixed spectral density viewed through a window.

$$\begin{aligned} \tilde{x}(t) &= w(t)\tilde{g}(t) \\ x(t) &= w(t)g(t) \end{aligned} \tag{41}$$

where $x(t)$ is a realization of the random process, $\tilde{x}(t)$, $w(t)$ is a deterministic window, and $g(t)$ is a realization of a dimensionless stationary random process, $\tilde{g}(t)$, with unity variance and mean μ_x.

Variance of Temporal Moments

Variance of Basic Moments. Later we will estimate the temporal moments to characterize transients with a large random component. It will be useful to have a measure of the variance of these estimates. In general we cannot find the variance without a model for the nonstationary process. All nonstationary processes obviously do not fit the product model, but the assumption of the

product model will lead to useful estimates of the variance.

In this section we will assume that $x(t)$ is a realization of a nonstationary random process, $\tilde{x}(t)$. The random process possesses a well-defined specification, and this specification includes finite values for the expected values of all finite temporal moments.

If the time history contains a random component, only estimates of the temporal moments can be made. For most of this article it will be assumed that only one realization of the process is available. A short discussion at the end will discuss the handling of more than one realization. The estimator for the ith temporal moment about a is given by

$$\hat{m}_i(a) = \int_{-\infty}^{\infty} (t - a)^i \, x^2(t) \, dt. \tag{42}$$

The expected value of the ith temporal moment is given by

$$E[m_i(a)] = \int_{-\infty}^{\infty} (t - a)^i \, E[\tilde{x}^2(t)] \, dt \tag{43}$$

E[ ] is the expectation operator, not energy. It can be seen that the estimate of the temporal moments given by Eq. (42) is unbiased by taking the expected value of Eq. (42) and comparing it with Eq. (43).

$$E[\hat{m}_i(a)] = E[m_i(a)]. \tag{44}$$

The variance of a temporal moment about 0 is given by

$$\text{var}[\hat{m}_i] = E[(\hat{m}_i - E[m_i])^2] = E[\hat{m}_i^2] - E[m_i]^2. \tag{45}$$

Combining Eqs. (43) and (45) for $a = 0$ gives

$$\text{var}[\hat{m}_i] = \int_{-\infty}^{\infty} \int_{-\infty}^{\infty} t^i s^i E[\tilde{x}^2(t)\tilde{x}^2(s)] dt \, ds \; - E[m_i]^2. \tag{46}$$

If we assume the product model, the variance can be written as

$$\text{var}[\hat{m}_i] = \int_{-\infty}^{\infty} \int_{-\infty}^{\infty} t^i s^i w^2(t) w^2(s) E[\tilde{g}^2(t)\tilde{g}^2(s)] \, dt \, ds - E[m_i]^2. \tag{47}$$

When the stationary random process, $g(t)$, in Eq. (41) is normally distributed, the expected value of the g product in the above equation can be written as (Bendat and Piersol, 1986, p. 260)

$$\begin{aligned} E[\tilde{g}^2(t)\tilde{g}^2(s)] &= 2(R_{gg}^2 \, (t - s) - \mu_g^4) + \psi_g^4 \\ &= 2(C_{gg}^2 \, (t - s) + 2\mu_g^2 C_{gg}(t - s)] \\ &\quad + \psi_g^4 \end{aligned} \tag{48}$$

where

$$R_{gg}(\tau) = E[\tilde{g}(t)\tilde{g}(t + \tau)], \quad \text{the autocorrelation function of } g(t) \tag{49}$$

$$C_{gg}(\tau) = E[(\tilde{g}(t) - \mu_g)(\tilde{g}(t + \tau) - \mu_g)], \quad \text{the autocovariance of g(t)} \tag{50}$$

$$\mu_g = E[\tilde{g}(t)], \quad \text{the mean of } \tilde{g}(t) \tag{51}$$

$$\psi_g^2 = E[\tilde{g}^2(t)], \quad \text{the mean square of } \tilde{g}(t). \tag{52}$$

Note

$$C_{gg}(\tau) = R_{gg}(\tau) - \mu_g^2. \tag{53}$$

Note also that

$$E[m_i]^2 = \psi_g^4 \int_{-\infty}^{\infty} \int_{-\infty}^{\infty} t^i s^i w^2(t) w^2(s) \, dt \, ds. \tag{54}$$

Substituting Eqs. (48) and (54) into Eq. (47), and letting $t = \tau + s$ gives

$$\text{var}[\hat{m}_i] = 2 \int_{-\infty}^{\infty} (C_{gg}^2(\tau) + 2\mu_g^2 C_{gg}(\tau)) \int_{-\infty}^{\infty} ((\tau + s)^i \, w^2(\tau + s) s^i w^2(s)) \, ds \, d\tau. \tag{55}$$

Let

$$W_{ii}(\tau) = \int_{-\infty}^{\infty} (\tau + s)^i \, w^2(\tau + s) s^i w^2(s) \, ds. \tag{56}$$

Note that by letting

$$z(t) = t^i w^2(t) \tag{57}$$

and where $Z(\omega)$ equals the Fourier transform of $z(t)$

$$Z(\omega) = F\{z(t)\} \tag{58}$$

then

$$W_{ii}(\tau) = F^{-1}\{Z(\omega)Z^*(\omega)\}. \tag{59}$$

When $w(t)$ is known, using the FFT and being careful to avoid circular convolution errors, Eqs. (57–(59) become a very convenient way to evaluate Eq. (56).

Substituting Eq. (56) into Eq. (55) gives

$$\text{var}[\hat{m}_i] = 2\int_{-\infty}^{\infty} W_{ii}(\tau)[C_{gg}^2(\tau) + 2\mu_g^2 C_{gg}(\tau)]\,d\tau. \tag{60}$$

Thus we see that the temporal moment variance is the integral of the product of two functions. The first is a function only of the deterministic window, and the second is a function of the mean and covariance of the random part of the model. This is a useful and general result for the product model.

Variance of Functions of Temporal Moments. We can directly compute the estimates of the temporal moments, $\hat{m}_i$, from Eq. (1), and estimates of the variance of the temporal moments estimators from Eq. (60), but we also would like estimates of the variance of functions of the estimated temporal moments. The functions of principal interest were previously defined and include: the energy, E; the centroid, τ; the rms duration, D; the skewness, S_t; the normalized skewness, S; the kurtosis, K_t; the normalized kurtosis, K; and the root energy amplitude, A_e.

We can approximate the variances of these functions with the following technique. Let h be one of the functions of the estimated temporal moments

$$h(\hat{m}_0, \hat{m}_1, \ldots, \hat{m}_n). \tag{61}$$

Expand this function with a Taylor's series about its mean

$$h(\hat{m}_0, \hat{m}_1, \ldots, \hat{m}_n) = h(\mu) + \sum_{j=0}^{n} (\hat{m}_j - \mu_j)\frac{\partial h}{\partial \hat{m}_j} + \text{higher terms} \tag{62}$$

where μ is the mean of the function h and μ_j is the $E[\hat{m}_j]$. The variance of h is given by

$$\text{var}[h] = E[(h - h(\mu))^2]. \tag{63}$$

Substituting Eq. (62) into Eq. (63) and neglecting the higher terms gives the first order approximation

$$\text{var}[h] \approx \sum_{j=0}^{n}\sum_{k=0}^{n} E[(\hat{m}_j - \mu_j)(\hat{m}_k - \mu_k)]\frac{\partial h}{\partial \hat{m}_j}\frac{\partial h}{\partial \hat{m}_k}. \tag{64}$$

Using the same technique that was used to derive Eq. (60), it can be shown that the covariance between $\hat{m}_j$ and $\hat{m}_k$ is given by

$$\begin{aligned}\text{cov}[\hat{m}_j, \hat{m}_k] &= E[(\hat{m}_j - \mu_j)(\hat{m}_k - \mu_k)] \\ &= 2\int_{-\infty}^{\infty} W_{jk}(\tau)(C_{gg}^2(\tau) \\ &\quad + 2\mu_g^2 C_{gg}(\tau))\,d\tau\end{aligned} \tag{65}$$

where

$$W_{jk}(\tau) = \int_{-\infty}^{\infty} (t + \tau)^j w^2(t + \tau) t^k w^2(t)\,dt. \tag{66}$$

The special form for $\tau = 0$, is

$$W_{ij} = W_{ij}(0) = \int_{-\infty}^{\infty} t^{j+k} w^4(t)\,dt. \tag{67}$$

We can write Eq. (64) in the form of a matrix where

$$\mathbf{p} = \left[\frac{\partial h}{\partial \hat{m}_0}\frac{\partial h}{\partial \hat{m}_1}\cdots\frac{\partial h}{\partial \hat{m}_n}\right]^T \tag{68}$$

$$\mathbf{C} = \begin{bmatrix} \text{cov}(\hat{m}_0, \hat{m}_0)\text{cov}(\hat{m}_0, \hat{m}_1) \cdots \text{cov}(\hat{m}_0, \hat{m}_n) \\ \text{cov}(\hat{m}_1, \hat{m}_0) \quad \cdots \\ \vdots \\ \text{cov}(\hat{m}_n, \hat{m}_0) \quad \cdots \quad \text{cov}(\hat{m}_n, \hat{m}_n) \end{bmatrix} \tag{69}$$

$$\text{var}[h] = \mathbf{p}^T\mathbf{C}\mathbf{p}. \tag{70}$$

Remember that Eq. (70) is a first order approximation.

Special Case Where Bandwidth of Underlying Process Is Large. An important special case is when the bandwidth of the underlying random process, $\tilde{g}(t)$, is large, such that of the autocorrelation function of $\tilde{g}(t)$, $R_{gg}(t)$, becomes small in a time that is short compared with the duration of the window, $w(t)$.

For this case Eqs. (60) and (65) become

$$\text{var}[\hat{m}_i] \approx 2W_{ii} \int_{-\infty}^{\infty} (C_{gg}^2(\tau) + 2\mu_g^2 C_{gg}(\tau))\, d\tau \tag{71}$$

$$\text{cov}[\hat{m}_i, \hat{m}_j] \approx 2W_{ij} \int_{-\infty}^{\infty} (C_{gg}^2(\tau) + 2\mu_g^2 C_{gg}(\tau))\, d\tau. \tag{72}$$

The integral parts of Eqs. (71) and (72) have units of time because $\tilde{g}(t)$ is a dimensionless random variable with unity variance. This integral can be expressed as an equivalent reciprocal bandwidth,

$$\frac{1}{B_{\text{eq}}} = 2 \int_{-\infty}^{\infty} (C_{gg}^2(\tau) + 2\mu^2{}_g C_{gg}(\tau))\, d\tau. \tag{73}$$

Equations (71) and (72) become

$$\text{var}[\hat{m}_i] \approx W_{ii}/B_{eq} \tag{74}$$

$$\text{cov}[\hat{m}_i, \hat{m}_j] \approx W_{ij}/B_{eq} \tag{75}$$

and the variance becomes

$$\text{var}[h] = \frac{\mathbf{p}^T \mathbf{W} \mathbf{p}}{B_{\text{eq}}} \tag{76}$$

where

$$\mathbf{W} = \begin{bmatrix} W_{00} & W_{01} & \cdots & W_{0n} \\ W_{10} & \cdots & & \\ \vdots & & & \\ W_{n0} & \cdots & & W_{nn} \end{bmatrix}. \tag{77}$$

The units of the product $p^T W p$ will be (units of the function $h)^2$/time.

Equation (76) is a very useful result. The variance is expressed as the ratio of two functions. The numerator does not depend on the underlying random process, but depends on the temporal moment order, the deterministic window, and on the partial derivatives of the function h with respect to the temporal moments. The denominator is an equivalent bandwidth that is a function of only the underlying random process.

General Case of Nondimensional Error Measures. Consider a nondimensional measure of the error, e

$$e^2 = \frac{\text{var}[h]}{h^2}. \tag{78}$$

As shown above, for large bandwidths of the random process, $\tilde{g}(t)$, this error measure will always be proportional to the inverse of the product of an equivalent bandwidth of the random process and an equivalent time parameter.

Let

$$\frac{1}{T_{eq}} = \frac{\mathbf{p}^T \mathbf{W} \mathbf{p}}{h^2}. \tag{79}$$

T_{eq} can be thought of as an equivalent averaging time for the window and the temporal function being estimated. Combining Eqs. (76), (78), and (79) we get the familiar form

$$e = \frac{1}{\sqrt{B_{\text{eq}} T_{\text{eq}}}}. \tag{80}$$

For large bandwidths, these error measures, e, when plotted on a log–log graph as a function of the $B_{\text{eq}}T_{\text{eq}}$ product will be a straight lines with a slope of $-1/2$. Comparing Eqs. (60) and (71), and noting that the maximum of $W_{ii}(\tau)$ is W_{ii}, reveals that Eq. (80) overestimates the error for smaller bandwidths, and is hence a conservative result.

A word of caution is needed. For the odd temporal moments the denominator of Eq. (78) can be 0, and the nondimensional error measure, e, becomes undefined. An example is the centroid, τ, or the skewness, S or S_t. It is then necessary to look at the variance directly instead of the error, e.

To evaluate Eq. (80) we need measures for estimates of B_{eq} and T_{eq}. Recall that the equivalent bandwidth, B_{eq}, is a function of the underlying stationary random process only, and the equivalent averaging time, T_{eq}, is a function of the temporal moment function and the window only. An estimate of B_{eq} is determined from an estimate of the covariance and mean of the underlying random process, $g(t)$, and Eq. (73). A crude estimate of the autocorrelation, and hence, the covariance [using Eq. (53)] can be made from the inverse Fourier transform of the Fourier energy spectrum. If the transient is divided into bandwidths using bandpass filters, a common assumption is that the spectrum is flat within the bandwidth, and hence, the bandwidth used is just the bandwidth of the filter. The mean is often assumed to be 0. The mean can also be estimated from the data, $x(t)$.

To evaluate T_{eq} we must evaluate Eq. (79), which means that we must have values for **p**, **W**, and **h**. The vector, **p**, is a sensitivity vector, relat-

ing how the variance of a function of the temporal moments, h, varies with a change in each of the temporal moments, m_i, in turn. Equation (68) defines the vector. Examples are given in Appendix C. The elements of the matrix **W** can be evaluated from Eq. (67) if the window is known, or estimated if the window is unknown as follows,

$$E\left(\int_{-\infty}^{\infty} t^{i+j}|x(t)|^4 dt\right) = W_{ij}E[\tilde{g}^4(t)]. \quad (81)$$

The expected value $E[x^4(t)]$ is a constant, and can be assumed unity. Thus we can use the equation

$$\hat{W}_{ij} = \int_{-\infty}^{\infty} t^{i+j}|x(t)|^4 dt \quad (82)$$

to estimate the elements of **W** if the window is not known. Similarly we can use the estimate of $\hat{h}^2$, computed from estimates of the temporal moments for h^2 in Eq. (79), to estimate T_{eq}.

T_{eq} is tabulated for example windows and the desired functions of the temporal moments in Appendix B. If the window can be approximated by one of the windows in Appendix B, T_{eq} can be approximated by one of the values in the appendix.

Special Case where Underlying Process, g(t), is Bandlimited White Noise, and Window Is Rectangular of Length T. For the special case where $\tilde{g}(t)$ is bandlimited white noise with 0 mean, the autocorrelation of $\tilde{g}(t)$ is given by Bendat and Piersol (1986, p. 114),

$$R_{gg}(\tau) = \frac{\sin(2\pi B\tau)}{2\pi B\tau} \quad (83)$$

$$B_{eq} = B \quad (84)$$

$$w(t) = \begin{cases} 1 & 0 \le t \le T \\ 0 & \text{elsewhere.} \end{cases} \quad (85)$$

From Eq. (67)

$$W_{00}(t) = T\left(1 - \frac{|t|}{T}\right) \quad -T \le t \le T \quad (86)$$

$$= 0 \qquad \text{elsewhere}$$

$$W_{00} = T. \quad (87)$$

The variance of the energy, using Eq. (60), becomes

$$\text{Var}[E] = 2T\int_{-T}^{T}\left(1 - \frac{|\tau|}{T}\right)(C_{gg}^2(\tau) + 2\mu_g^2 C_{gg}(\tau))\, d\tau. \quad (88)$$

From Eqs. (1) and (5), the energy, E, is $1/T$. The normalized variance of the energy is then

$$e_E^2 = \frac{\text{Var}[E]}{E^2} = \frac{2}{T}\int_{-T}^{T}\left(1 - \frac{|\tau|}{T}\right)(C_{gg}^2(\tau) + 2\mu_g^2 C_{gg}(\tau))\, d\tau \quad (89)$$

which is Eq. 8.40 in Bendat and Piersol (1986, p. 260) for the variance of a single sample time history from a stationary (ergodic) random process with a unity mean square value. Thus we see that Eq. 8.40 in Bendat and Piersol is a special case of Eq. (60).

Using the value for $T_{eq} = T$ from Appendix B we get

$$e_E^2 \approx \frac{1}{BT} \quad (90)$$

which is equivalent to Eq. 8.58 in Bendat and Piersol (1986, p. 263). As before, Eq. 8.58 in Bendat and Piersol is a special case of Eq. (80).

This is a fairly general result. The errors for other temporal moments, and other functions of the temporal moments, will have the same general characteristics. Equation (80) showed that all the desired functions of the temporal moments will have the same form at large bandwidths. The error will be a straight line with a slope of $-1/2$ on a log–log plot when plotted as a function of the product of a duration parameter and a bandwidth parameter. At smaller bandwidths the error estimated with the large bandwidth assumption will always be larger than the actual error. The product of the bandwidth and rms duration needs to be only greater than about 5 for the large bandwidth approximation to be very useful. This implies that the values in Appendix B for T_{eq} and Eq. (80) will yield useful approximations for the errors in most practical problems.

Variance Estimates when More than One Realization is Available. When more than one realization is available, the temporal moments for each realization can be calculated. The resulting estimates can then be averaged. This should result in a variance reduction of the estimates by $1/N$ where N is the number of realizations avail-

able. This is the only practical way to reduce the variance of the moment estimates. If only one or a few realizations are available, the bandwidth of the analysis must be restricted to values that will yield statistically significant results.

APPLICATIONS TO TRANSIENT VIBRATIONS

For the remainder of the discussion the time history will be taken as an acceleration time history. With minor modifications the discussions could also apply to velocity, displacement, strain, force, or any other measure of vibration.

The method proposed in this article models the shock as

$$x(t) = x_m(t) + x_r(t) \tag{91}$$

where, $x(t)$ is the shock being characterized, $x_m(t)$ is the mean shock that contains the velocity change information and the deterministic part of the shock, and $x_r(t)$ is the shock with the mean removed, the nondeterministic or random part of the shock. $x_r(t)$ will be modeled later with the product model.

The mean shock is found by ensemble averaging the individual shocks to estimate the deterministic part of the shock. If multiple records are not available for ensemble averaging, a deterministic model for $x_m(t)$ with the correct velocity change can be assumed, or the mean shock can be assumed to be 0 (which assumes a velocity change of 0). The mean shock is then subtracted from each ensemble record leaving a zero mean time history, x_r. Note, if an ensemble average is used, a zero mean in this context is stronger than saying the time history has a zero first integral or zero velocity change. It implies that the expected value of every point in time of the ensemble average is 0. The mean computed for a particular record will still not necessarily have a zero mean because of the uncertainty of the mean from a single realization. If this causes a problem, a slight modification of the procedure can subtract the sample mean instead of the ensemble mean from each record. The ensemble energy spectrum of zero mean time histories, $x_r(t)$, is estimated by averaging the magnitude squared of the Fourier spectra of all records,

$$|\bar{X}_r(\omega)|^2 = \frac{1}{n} \sum_n |X_r(\omega)|^2. \tag{92}$$

As discussed earlier, a significant problem exists when the Fourier energy spectrum is used to characterize a single time history: A lot of uncertainty exists in the spectrum, and the spectrum looks "noisy." This will be illustrated later. This objection can be overcome by smoothing the spectrum. One advantage of the SRS is that the shock is viewed through a SDOF filter that "smoothes" the spectrum. If we average adjacent frequency lines of the Fourier energy spectrum we can achieve similar results. If we do the smoothing on a basis where the filter bandwidth is proportional to the center frequency we can preserve the low frequency character of the waveform while significantly smoothing the higher frequency "noise" in the spectrum. This is very much like the shock intensity spectrum defined by Baca (1989) and gives a "smoothness" very much like the SRS. This will be illustrated by example later. The smoothed average is defined as

$$|\bar{X}(\omega)|^2 = \frac{1}{\Delta} \sum_{\omega-\Delta/2}^{\omega+\Delta/2} |X(\omega)|^2 \, d\omega \tag{93}$$

where Δ is the bandwidth of the smoothing filter. A combination of averaging, Eq. (92), and smoothing, Eq. (93), can be used when a few records are available.

The zero mean time histories, $x_r(t)$, are then filtered with a set of N contiguous band-pass filters. In some cases for the analysis of transient data the mean is not removed. For these cases the first filter is a low pass filter, and the mean response is contained in this band limited time history. As explained earlier the uncertainty theorem and the variance of the temporal moment estimates limits the bandwidth of these filters. The output of each filter is then characterized using the first four or five normalized central moments of the band-passed time history; the energy, E (or the root energy amplitude, A_e); the location of the centroid, τ; the rms duration, D; the skewness, S; and optionally the kurtosis, K. For transient time histories these moments and the smoothed Fourier energy spectrum should give an adequate description of the data. By dividing the data into bandwidths, the transient is described in both time and frequency. The number of moments and the number of frequency bands is kept small so that statistically significant statements can be made about the parameters with a limited amount of data.

In summary the shock is characterized by:

1. a mean shock that characterizes the velocity change and any deterministic part of the shock;
2. an averaged or smoothed Fourier energy spectrum that characterizes how the energy is distributed in frequency;
3. band limited temporal moments, E, A_e, τ, D, S, and K that characterize how the energy is distributed in time and frequency.

Test conservatism can now be objectively evaluated. The energy spectrum, the band limited energy or REA can be evaluated. The variance of these quantities can be estimated. Conservatism is controlled primarily through these energy measures, because of their linear nature. If all other things are held constant, raising the energy by a factor of four, or REA by two, will raise the response by a factor of two. Envelopes of different but similar events can be formed. The energy of the envelope will be conservative when compared with the underlying spectra.

The temporal moments describe how the energy is distributed in time. Values for these functions and their variance can be estimated. The change in response to variations in the moments can be described qualitatively, but a nice linear relationship, as for energy, does not exist for the higher moments. Decreasing the rms duration, D, typically produces higher responses because the same energy is applied in a shorter time. However, the increase is not linear. If the duration of the waveform is short compared to the period of the test item, the input looks like an impulse to the system. Making the input shorter will not significantly increase the response. Keeping the rms duration of the test shock equal or shorter than the environment will typically produce a conservative result. A similar skewness will imply that the rise and fall times of the test transient will be about the same as the use environment. A similar skewness should produce a similar response. As the absolute value of the skewness increases, the time history tends to have a sharper rise time or fall time that tends to produce a larger peak response. The role of kurtosis is less well understood. Kurtosis tells us something about the "peakedness" of the data envelope, and may be useful for data that has an envelope with more than one peak. If the envelope is shaped like a normal distribution curve the kurtosis will be 3. As the area of the window is more concentrated toward the center the kurtosis becomes smaller. As the area is spread toward the tails, becoming even bimodal, the kurtosis increases. The kurtosis for several common waveforms is given in Appendix B. It may also be useful for those environments where the duration is long compared to the impulse response time of a system exposed to the environment. In this case the transient starts to look like nonstationary vibration and the kurtosis gives us some information about the peak to rms ratio.

Conservatism is controlled primarily with the energy spectrum. The centroidal times, τ, the rms duration, D, the skewness, S, and the kurtosis, K, should be kept as close to the actual environment as possible. To produce a more conservative test than the field environment one should; make the energy larger; make the rms durations shorter; make the absolute value of the skewness larger; and make the kurtosis smaller. Two examples in the next section will illustrate the method.

Use of SRS to Replace Energy Spectrum

Note that the shock response spectrum could be substituted for the energy spectrum, but this is not recommended. The band limited temporal moments would then serve as additional information about the shock to further quantify the environment, and to restrict the class of waveforms that could be used to simulate the environment. In this case the energy in each band must be included to calculate the normalized central moments. This method removes the simplicity of the energy spectrum, complicates the synthesis of test realizations, and test conservatism becomes more difficult to evaluate. However, the method does retain the long history of the SRS as a characterization of a shock.

Example Characterization of a Projectile Shock

Characterization. Projectiles were instrumented with accelerometers, and fired, penetrating a hard target. Five accelerometer records from transducers mounted near the nose of the penetrator in the axial direction are discussed by Smallwood (1989). A typical record is shown as Fig. 1. The original data were digitized with a 50-kHz sample rate. The accelerometer for each record was mounted in the same location and in the same direction for the five different tests. The

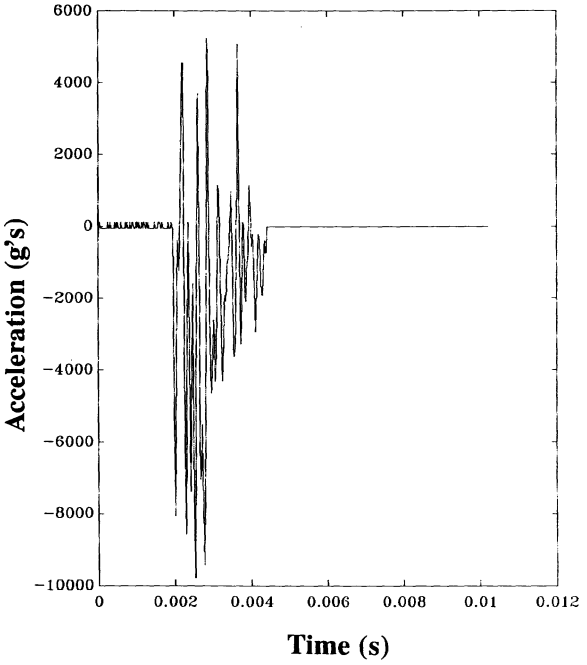

FIGURE 1 Penetration event 1.

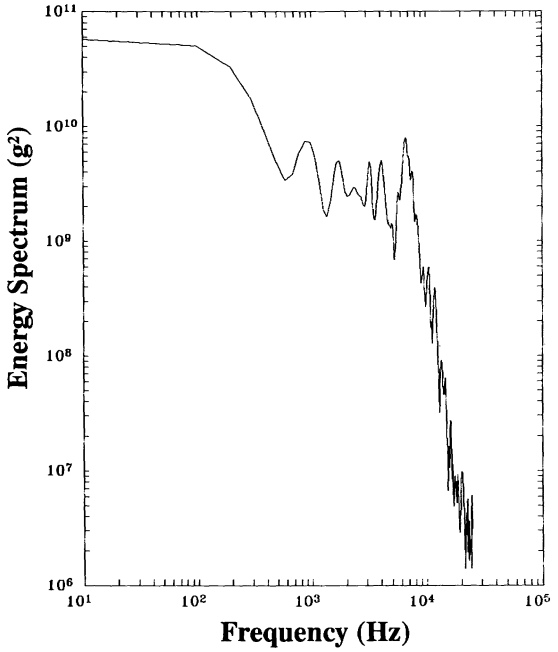

FIGURE 2 Average energy of the penetration events. Zero frequency plotted at 10 Hz for convenience. Zero value = 5.76×10^{10}.

records form an ensemble of five field events. The mean time history was calculated, but the high frequency random content was too large for an ensemble of five to have a meaningful mean shock. The mean shock showed a large variance. For the analysis the mean shock is included in the first band (0–2.5 kHz). Later in the simulation section a mean shock will be included as a deterministic waveform with the correct velocity change and temporal moments.

The energy was computed for each record by Smallwood (1989). The average energy was computed and is shown as Fig. 2. The units of energy in Fig. 2 are g^2 (not strickly energy, which would have units of g^2/Hz or g^2-s, because the spectrum was computed with an FFT that did not divide by the frequency resolution, g is the acceleration of gravity, 9.8 m/s^2). The velocity change can be determined from the value of the spectrum at 0 frequency (plotted at 10 Hz for convenience). The average velocity change from Fig. 2 is given by

$$\Delta v = \sqrt{5.76 \times 10^{10}/50{,}000} = 4.8g - \text{s} = 47\text{m/s}(150\text{ft/s}). \quad (94)$$

The penetrator did not stop during the event but slowed down by about 150 ft/s. The records were filtered with four filters: 0–2.5, 2.5–5, 5–7.5, and above 7.5 kHz. Narrower bandwidths are not statistically significant (Table 1).

Using the assumption that the equivalent bandwidth for a single transient is 10 kHz, the normalized errors can be estimated from Eq. (80) and are listed in Table 2. The standard deviations measured from the five measured events are also listed in Table 2 and are seen to be consistent with the estimated error. Decreasing the bandwidth by four to 2.5 kHz and increasing the number of events to five will decrease the estimated errors by the factor of only $\sqrt{4/5} \approx 0.9$ support-

Table 1. Moment Parameters Describing a Penetration Shock Environment

Property (ms)	Overall	Bandwidth (kHz) 0–2.5	2.5–5	5–7.5	>7.5
τ	2.5	3.6	3.6	3.6	3.4
	(0.5)	(0.5)	(0.4)	(0.6)	(0.6)
D	0.53	0.53	0.62	0.45	0.48
	(0.10)	(0.12)	(0.11)	(0.12)	(0.17)
S_t	0.52	0.46	0.56	0.11	0.52
	(0.11)	(0.14)	(0.17)	(0.39)	(0.11)

The first number in the table is the mean in milliseconds. The number in parentheses is the standard deviation in milliseconds.

Table 2. Normalized Errors for Penetrator Data

	Energy E	REA A_e	Centroid τ	rms Dur. D	Skewness S_t	Kurtosis K_t
Value	32k g^2s	8200 g	2.7 ms	0.48 ms	0.48 ms	0.68 ms
T_{eq}	0.7 ms	1.6 ms	1.4 ms	2.7 ms	0.4 ms	7 ms
e	40%	25%	27%	20%	50%	12%
Meas. SD			0.5 ms	0.1 ms	0.11 ms	

g is the acceleration of gravity, 9.8 m/s^2.

ing the argument for bandwidths of at least 2.5 kHz.

The moment parameters for each record in each bandwidth were then computed. The parameters were averaged across the ensemble of five events and the results are listed in Table 3. The energy and REA are not included in Table 3 because this information is included in the Fourier energy spectrum. For this example the kurtosis was not considered. For this environment a strong dependence on frequency is not evident. Simulation of the environment using the overall unfiltered parameters would not be unreasonable. This is supported by the variance estimates given in Table 2. However, the frequency dependent parameters are retained to illustrate the method. The skewness parameter is always positive indicating a fast rise time and a slower decay time consistent with a casual observation of the data. It does illustrate the value of including the third moment. The energy spectra along with the table of normalized central temporal moments give a good representation of this environment.

Simulation Using Product Model of Nonstationary Random Vibration. The penetrator event was simulated (Smallwood, 1989) using the product model. A pulse of the form

$$w(t) = A(t^n - T^{n-p}t^p). \qquad (95)$$

was used as the window and to simulate the portion of the event that includes the velocity change, $x_m(t)$. The waveform shown in the equation above was reversed to give a positive skewness. The parameters A, T, n, and p for $x_m(t)$ were chosen to match the energy and the temporal moments of the overall unfiltered mean event. The stationary random process used for the random portion of the product model had the same spectrum as the mean spectrum of the five events. This assured matching of the energy. The parameters A, T, n, and p were chosen for each bandwidth to match the properties in Table 3. A typical realization is shown as Fig. 3. For comparison the average SRS of the five field events and the average SRS of five simulations is shown in Fig. 4.

Adjacent Missile Firing on an External Store

Characterization. The response of an adjacent store to the firing of an AIM 120 (AMRAAM) missile will now be described in three different ways and compared. The first method will use the SRS. The second method will use a nonstationary vibration model to describe the event. The third method will use the band-limited temporal moments described above. The response to the adjacent missile firing was measured at several locations in three axes, but a single accelerometer in a single axis will be used for the com-

Table 3. Normalized Central Temporal Moments for Penetration Data

Property ms	Overall	0–2.5 kHz	2.5–5 kHz	5–7.5 kHz	>7.5 kHz
τ	2.5	3.6	3.6	3.6	3.4
	(0.5)	(0.5)	(0.4)	(0.6)	(0.6)
D	0.53	0.53	0.62	0.45	0.48
	(0.10)	(0.12)	(0.11)	(0.12)	(0.17)
S_t	0.52	0.46	0.56	0.11	0.52
	(0.11)	(0.14)	(0.17)	(0.39)	(0.11)

The first number on the table is the mean. The number in parentheses is the standard deviation.

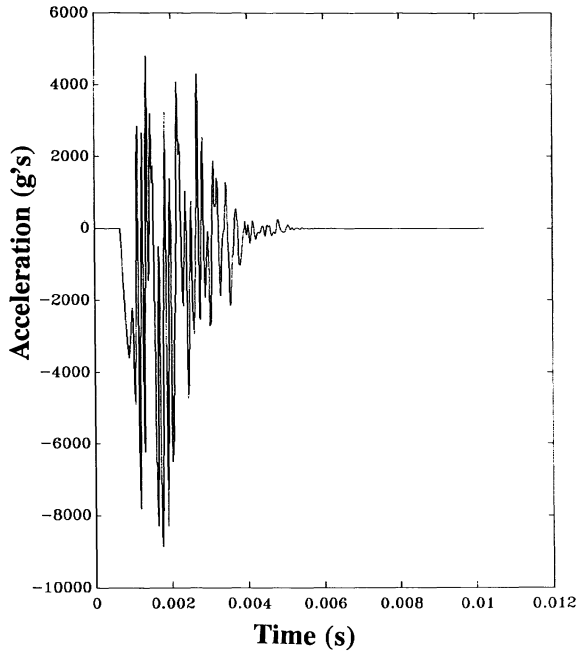

FIGURE 3 One realization of the penetration event simulation.

parison here. The location chosen is a component located near the nose of the external store at a location away from the skin, but not isolated from the skin. The axis chosen is the transverse axis of the store and the aircraft. A typical time history of the event for this accelerometer is shown as Fig. 5. The short-term time averaged rms is also shown in Fig. 5.

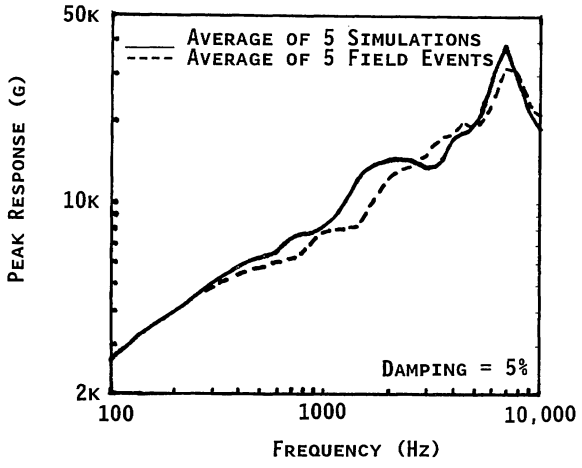

FIGURE 4 Comparison of the SRS, the mean penetration event, and the average SRS of five penetration simulations.

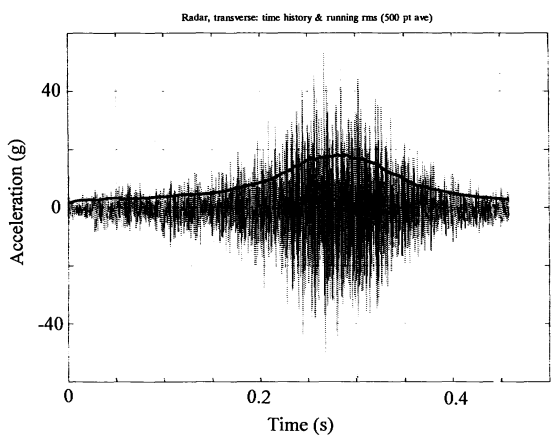

FIGURE 5 Time history of the response in and the time averaged rms of the missile firing event.

The short-term time averaged rms is defined as

$$\bar{x}^2(t) = \frac{1}{\delta} \sum_{t-\delta/2}^{t+\delta/2} x^2(t)dt. \tag{96}$$

For this example δ was 0.048 s. The SRS of the field event is shown as the solid curve with x's on Fig. 6. The other curves will be explained later.

For the second method the autospectral density was computed in two ways. First the spectrum was computed in the usual way using Welch's method ignoring the nonstationary nature of the data. The sample rate of the data was 10417 samples/s. The data were filtered with a 4-kHz lowpass filter. The total record was 4778 samples (0.4587 s). The data were analyzed with

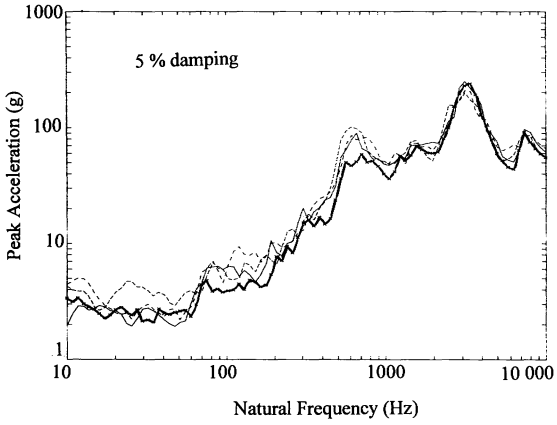

FIGURE 6 SRS of the time history of Fig. 5 and three simulations.

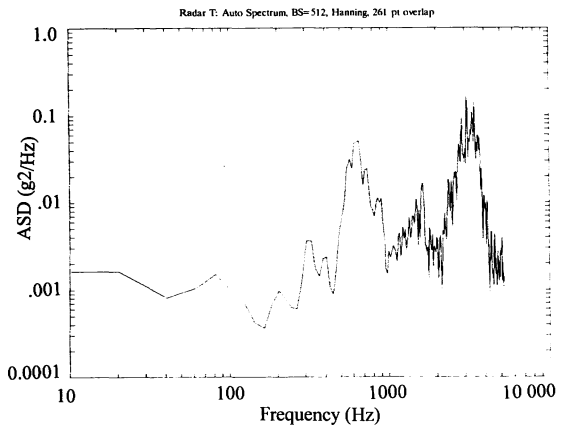

FIGURE 7 Autospectrum of the time history of Fig. 5.

a Hanning window, a block size of 512 with a 261 point overlap. This result is shown as Fig. 7. This procedure might introduce some bias error, but the procedure is commonly done and is used for comparison with the other procedures. Next the acceleration was divided by the time averaged rms (called the running average, and shown in Fig. 5) to convert the time history into a pseudo-stationary process with a unity rms. The autospectrum of this time history was computed with the same analysis parameters as the previous spectrum. This result is Fig. 8. If the product model is correct we would expect these two spectra shapes to be the same within the statistical error. We see that this is generally true except for an excess of high frequency energy above 2 kHz in the original spectrum (compare Figs. 7 and 8). The normalization process gives more weight to the low levels at the beginning and end of the time history. This suggests that the product model is not quite correct, and that the adjacent missile firing excites more high frequencies than the background vibration present before and after the firing. If the product model can be assumed, the autospectrum and the running rms give a fairly complete description of the event. The only weakness is the lack of frequency resolution necessitated by the requirement for a reasonable Bandwidth-Averaging Time (BT) product to keep the statistical error at a reasonable value. This can be improved if more than one realization of the event is available and ensemble averaging can be used.

The Fourier energy spectrum is shown as Fig. 9. Notice the large uncertainty in this data as previously alluded to. The spectrum was smoothed by averaging the frequencies over a bandwidth 16% of the center frequency. This is comparable to the bandwidth of the SDOF filter used in the SRS analysis. The result is shown as Fig. 10. Note that the spectrum shape is very similar to the previous autospectrum if the difference in frequency resolution is considered. Thus, as expected, the autospectrum and the Fourier energy spectrum contain much the same information. Note that the SRS does not contain quite the same information. As above, the frequency resolution can be improved if ensemble averaging can be used.

The temporal moments for the acceleration time history filtered into approximate 1/3 octave bandwidths are shown as Figs. 11 and 12. The energy, E, and the root energy amplitude, A_e, are shown in Fig. 11. Note that these functions con-

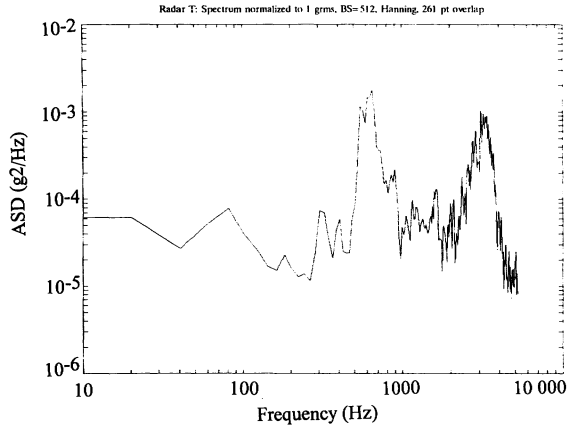

FIGURE 8 Normalized autospectral density of the time history of Fig. 5.

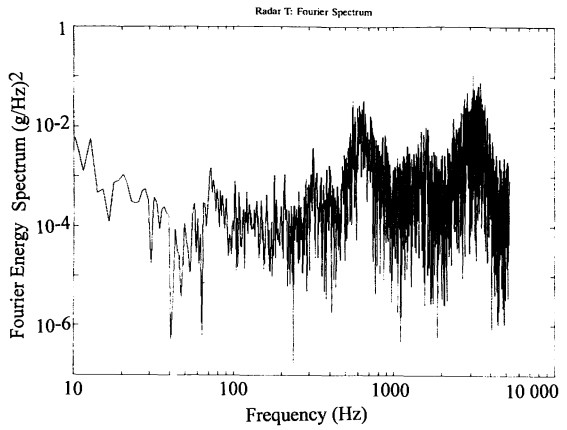

FIGURE 9 Fourier energy spectrum of the time history of Fig. 5.

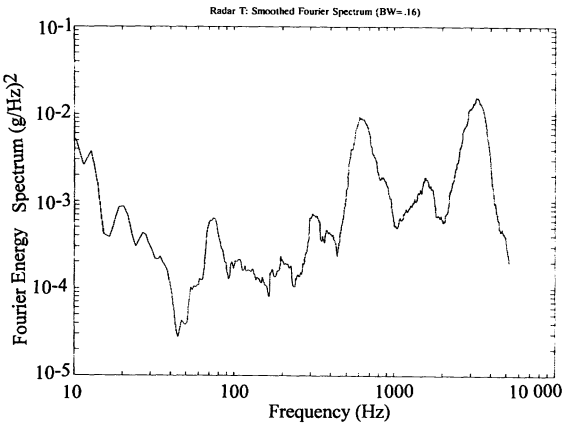

FIGURE 10 Smoothed Fourier energy spectrum of the time history of Fig. 5.

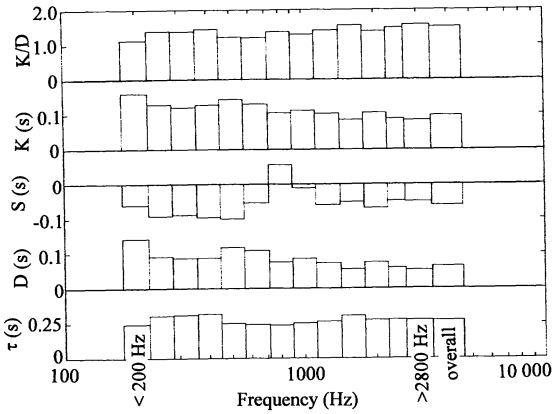

FIGURE 12 Normalized temporal moments of the time history of Fig. 5.

tain much the same information as the autospectra and the Fourier energy spectra. Just as for the other spectra the frequency resolution could be improved by using a narrower filter at the expense of statistical accuracy. If the product model is correct, the normalized central temporal averages (τ, D, S, and K) (Fig. 12) should be independent of frequency except for statistical errors. The uncertainty of the moments can be estimated using the results of the previous sections. For comparison, the parameters for a rectangular window of duration 0.4587 s are: τ = 0.229 s, D = 0.132 s, S = 0, K_t = 0.153 s, and $K = K_t/D = 1.15$.

In Fig. 12 the first values plotted at 200 Hz are the values for a low pass filter with a cutoff frequency of 200 Hz. The next to the last value plotted at 3000 Hz are the values for a high pass filter with a cutoff frequency of 2800 Hz. The last value plotted at 4000 Hz are the values for the overall unfiltered waveform.

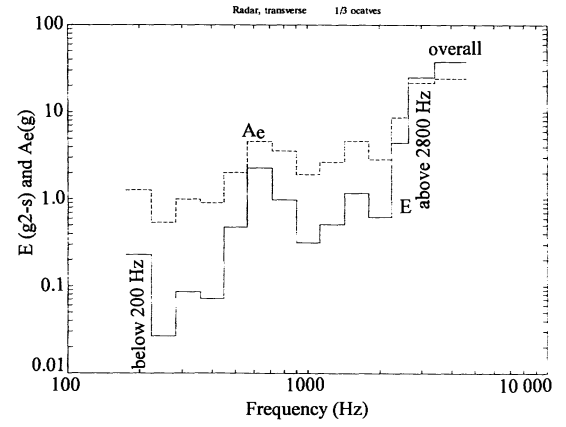

FIGURE 11 Energy and root energy amplitude of the time history of Fig. 5.

The centroid of the data is reasonably independent of frequency. The rms duration shows a systematic decrease as the frequency increases; this suggests that the product model based on the overall parameters is not quite correct. The data suggests that the high frequencies have a shorter duration than the low frequencies. This suggests that the excitation of the missile firing excites more high frequencies than the background excitation before and after the firing, which is consistent with the findings from the autospectrum data.

The skewness data show a much larger variation with frequency. It was expected that the statistical uncertainty would be larger than for the other normalized moments, but the variation is larger than expected. This has not been explained.

The kurtosis is more consistent (Fig. 12) and the ratio of the kurtosis to rms duration is almost constant. This indicates that the kurtosis also decreases with frequency along with the rms duration. This indicates that the data peaks are more centralized for the higher frequencies, again suggesting that the high amplitudes caused by the missile firing preferentially excite the high frequencies.

The frequency resolution of the band-limited temporal moments is not as good as the autospectrum or the Fourier spectrum, but they do provide temporal information missing from the spectra. The combination of the running rms and normalized autospectrum provides a good description of data for which the product model is

valid, but lacks the information giving the variation of temporal information as a function of frequency. A two-dimensional (time and frequency) spectral model might be appropriate if enough data are available to support the analysis.

Simulation. The adjacent missile firing was simulated with the product model, neglecting the observed changes in temporal moments with frequency. A window with the approximate temporal moments of the overall unfiltered waveform was used. The window was the sum of a rectangular window and a time shifted Hanning window. The window is shown as the solid line of Fig. 13. The stationary random signal was chosen to have the same spectrum as the smoothed Fourier spectrum of Fig. 10. A realization of this process is shown as Fig. 13.

The SRS of three simulations and the event of Fig. 5 are shown in Fig. 6. The most significant deviation between the simulations and the field event is in the area of 600–700 Hz. The simulations produced responses about 30% larger than the field data. Figures 14 and 15 show the response of a 661-Hz (one of the frequencies at which the SRS was calculated) SDOF system with 5% damping to the field event and the third simulation, respectively. As can be seen the response to the simulation is more concentrated around 0.25–0.35 s, where the response to the field event is more uniformly distributed over the whole frame of data. If we look back at Fig. 12, we see that the rms duration, D, was longer in this frequency band than was the overall rms duration, which was used in the simulation. Thus we would expect the rms duration of the simulation to be shorter than the rms duration of the field event in this frequency band, and because the energy is the same, the simulation should produce slightly larger responses, as observed. The change in rms duration detected a characteristic of the data not evident in either the autospectrum, the Fourier spectrum, or the SRS.

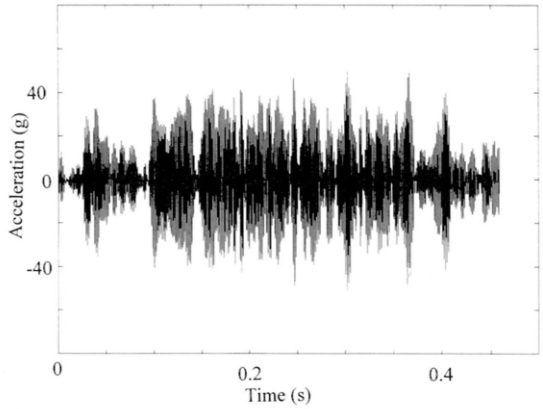

FIGURE 14 Response of a 661-Hz SDOF system with 5% damping to the input time history of Fig. 5.

CONCLUSIONS

The band-limited temporal moment method described offers significant advantages over other methods used to characterize shock environments. The method is particularly useful to describe oscillatory shocks. The method is simple and the characterization easy to interpret. The method uses functions (Fourier transforms and

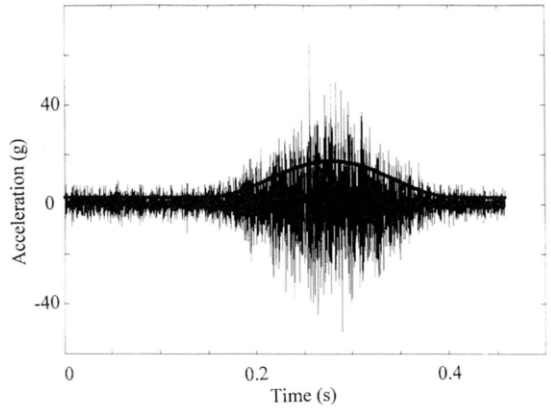

FIGURE 13 Realization of the simulation of the adjacent missile firing response of Fig. 5.

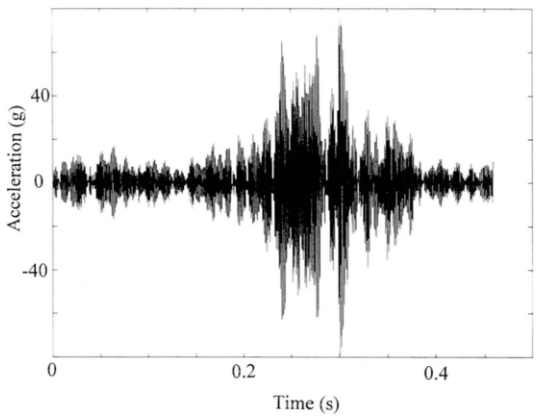

FIGURE 15 The response of a 661-Hz SDOF system with 5% damping to a simulation of the event of Fig. 5.

temporal moments) that are easy to implement. The method characterizes the shock and *not the response to the shock* (as does the SRS), and therefore does not depend on a structural model. The procedures lend themselves to a statistical treatment encouraging a probabilistic approach. It is shown that simulations can be generated that include the essential characteristics of the environment. Further work such as more comparisons with the method of shock response spectrum and other techniques need to be done. More examples and other windows need to be examined. A general procedure to develop windows that match specified moment parameters needs to be developed. This will aid the simulation process and allow studies to test the robustness of the procedure. The use of random parameters to modify the mean shock and windows should be developed.

This work was performed at Sandia National Laboratories and was supported by the U.S. Department of Energy under Contract DE-AC04-94AL85000.

REFERENCES

Baca, T. J., 1989, "Comparison of Shock Severity Measures," *60th Shock and Vibration Symposium,* SAVIAC, Arlington VA.

Bendat, J. S., and Piersol, A. G., 1986, *Random Data Analysis and Measurement Procedures,* 2nd ed., John Wiley & Sons, New York.

Chui, Charles K., 1992, *An Introduction to Wavelets,* Academic Press, Inc., San Diego, CA.

Hart, G. C., and Hasselman, T. K., 1976, "Estimation of Ship Parameters for Consistent Design and Test Specification," *Shock and Vibration Bulletin,* Vol. 46, pp. 155–167.

Himelblau, H., and Piersol A. G., 1989, "Evaluation Procedure for the Analysis of Nonstationary Vibroacoustic Data," *Journal of the Environmental Sciences,* Vol. 32, pp. 35–42.

Mark, W. D., 1972 "Characterization of Stochastic Transients and Transmission Media: The Method of Power-Moments Spectra," *Journal of Sound and Vibration* (1972) Vol. 22, No. 3, pp. 249–295.

Merritt, R. G., 1993, "Simulation of Ensemble Orientated Nonstationary Processes Part 1," *Proceedings of the Institute of Environmental Sciences,* Vol. 2, pp. 486–501.

Paez, T. L., and Baca, T. J., 1988, "Shaker Shock Testing Using Nonstationary Random Transients," *59th Shock and Vibration Symposium,* SAVIAC, Arlington, VA, Vol. 2, Sandia National Laboratories Report SAND88-2473C, UC-13.

Papoulis, A., 1962, *The Fourier Integral and Its Applications,* McGraw–Hill, New York.

Shinozuka, 1970, "Maximum Structural Response to Seismic Excitations," *Journal of the Engineering Mechanics Division, Proceedings of the American Society of Civil Engineers,* Oct., pp. 729–738.

Smallwood, D. O., 1973, "A Transient Vibration Test Technique Using Least Favorable Responses," *Shock and Vibration Bulletin,* No. 43, pp. 151–164.

Smallwood, D. O., 1975, "Time History Synthesis for Shock Testing on Shakers," *Seminar on Understanding Digital Control and Analysis in Vibration Test Systems,* Part 2, pp. 23–42, A Publication of the S&V Information Center, NRL, Washington DC. (Available from SAVIAC, Arlington, VA).

Smallwood, D. O., 1986, *Shock Testing on Shakers by Using Digital Control,* IES Technology Monograph, Mount Prospect, IL.

Smallwood, D. O., 1989, "Characterizing Transient Vibrations Using Band Limited Moments," *60th Shock and Vibration Symposium,* SAVIAC, Arlington, VA, Vol. 3, pp. 93–109.

APPENDIX A

Moments of Some Common Waveforms

Function	Δv	E	A_e	τ	D	S_t	S	K_t	K
Square wave $f(t) = 1$ $0 \le t \le T$	T	T	$\sqrt{2\sqrt[4]{3}}$ 1.86	$T/2$	$T/2\sqrt{3}$ $0.29T$	0	0	$T/2\sqrt[4]{5}$ $0.33T$	$\sqrt{3}/\sqrt[4]{5}$ 1.16
Triangle $f(t) = 1 - 2\frac{\lvert t\rvert}{T}$ $-T/2 \le t \le T/2$	$T/2$	$T/3$	$\sqrt{2\sqrt{10/3}}$ 1.45	$T/2$	$T/2\sqrt{10}$ $0.16T$	0	0	$T/2\sqrt[4]{35}$ $0.21T$	$\sqrt{10}/\sqrt[4]{35}$ 1.30
Half sine $f(t) = \sin(\pi t/T)$ $0 \le t \le T$	$2T/\pi$	$T/2$	$\sqrt{\frac{\pi\sqrt{3}}{\sqrt{\pi^2 - 6}}}$ 1.66	$T/2$	$T\sqrt{\frac{1}{12} - \frac{1}{2\pi^2}}$ $0.18T$	0	0	$0.225T$	1.17

Moments of Some Common Waveforms (continues)

Function	Δv	E	A_e	τ	D	S_t	S	K_t	K
Terminal peak sawtooth $f(t) = t/T$ $0 \le t \le T$	$T/2$	$T/3$	$\frac{\sqrt[4]{80}}{\sqrt{3\sqrt{3}}}$ 1.33	$3T/4$	$T\sqrt{\frac{3}{80}}$ $0.19T$	$-T/\sqrt[3]{160}$ $-0.18T$	$-\frac{\sqrt{80}}{\sqrt[3]{160}\sqrt{3}}$ -0.95	$0.257T$	1.32
Exponential $f(t) = e^{-\alpha t}$ $t \ge 0$	$1/\alpha$	$1/2\alpha$	1	$1/2\alpha$	$1/2\alpha$	$1/\sqrt[3]{4}\alpha$ $0.63/\alpha$	$\sqrt[3]{2}$ 1.26	$\frac{\sqrt{3}}{2\alpha}$ $0.866/\alpha$	$\sqrt{3}$ 1.73
$f(t) = t^n e^{-\alpha t}$ $t \ge 0$	$\frac{\Gamma(n+1)}{\alpha^{n+1}}$	$\frac{\Gamma(n+1)}{(2\alpha)^{2n+1}}$	$\sqrt{\frac{\Gamma(2n+1)}{(2\alpha)^{2n}(2n+1)}}$	$\frac{2n+1}{2\alpha}$	$\frac{\sqrt{2n+1}}{2\alpha}$	$\frac{\sqrt[3]{4n+2}}{2\alpha}$	$\frac{\sqrt[3]{2}}{\sqrt[6]{2n+1}}$		
$f(t) = t^n - T^{n-p}t^p$ $0 \le t \le T$	Δv_1	E_1	$\sqrt{E_1/D_1}$	τ_1	D_1	S_{t1}	S_{t1}/D_1		

Note: $\Gamma(2n+1) = (2n)!$ if n is an integer >0.

$$\Delta v = \int_{-\infty}^{\infty} f(t)dt \quad \Delta v_1 = T^{n+1}\left(\frac{1}{n+1} - \frac{1}{p+1}\right) \quad \bar{m}_j = \frac{1}{2n+j+1} - \frac{2}{n+p+j+1} + \frac{1}{2p+j+1}$$

$$E_1 = T^{2n+1}\bar{m}_0 \quad \tau_1 = T\bar{m}_1/\bar{m}_0 \quad D_1^2 = T^2\left(\frac{\bar{m}_2}{\bar{m}_0} - \frac{\bar{m}_1^2}{\bar{m}_0^2}\right) \quad S_{tt}^3 = T^3\left(\frac{\bar{m}_3}{\bar{m}_0} - \frac{3\bar{m}_1\bar{m}_2}{\bar{m}_0^2} + \frac{2\bar{m}_1^3}{\bar{m}_0^3}\right)$$

APPENDIX B

Equivalent Averaging Times for Several Common Windows and Several Common Functions of Temporal Moments

Window	Energy E	REA A_e	Centroid τ[a]	rms Duration D	Skewness S_t[b]	Kurtosis K_t
Rectangular $w(t) = 1$ $0 \le t \le T$	T	$3.33T$	T	$5T$	$0.49T$	$9T$
Triangle $0 \le t \le T$	$0.55T$	$1.3T$	$1.17T$	$2.6T$	$0.33T$	$6.4T$
Terminal peak sawtooth $0 \le t \le T$	$0.56T$	$1.6T$	$0.78T$	$3.8T$	$0.30T$	$7.3T$
Half sine $0 \le t \le T$	$0.67T$	$1.7T$	$1.1T$	$3.5T$	$0.34T$	$7.8T$
Hanning $0 \le t \le T$	$0.51T$	$1.3T$	$0.92T$	$2.7T$	$0.27T$	$6.3T$
Exponential $w(t) = e^{-\alpha t}$ $t \ge 0$	$1/\alpha$	$2.5/\alpha$	$2/\alpha$	$8/\alpha$	$0.44/\alpha$	$26.2/\alpha$
$w(t) = te^{-\alpha t}$ $t \ge 0$	$2.6/\alpha$	$6.4/\alpha$	$5.3/\alpha$	$16/\alpha$	$1.2/\alpha$	$40/\alpha$

[a]For this odd temporal moment T_{eq} corresponding to $e^2 = \text{var}[\tau]/D^2$ is given.
[b]For this odd temporal moment T_{eq} corresponding to $e^2 = \text{var}[S_t^2]/D^6$ is given.

APPENDIX C

Listing of Vectors, *p*, for Commonly Desired Functions of Temporal Moments

Energy, E

$$\mathbf{p}_E = 1. \tag{C.1}$$

Centroid, τ

$$\mathbf{p}_\tau = [-m_1/m_0^2 \quad 1/m_0]^T \tag{C.2}$$

rms duration squared, D^2

$$\mathbf{p}_{D^2} = [(-m_2/m_0^2 + 2m_1^2/m_0^3)\ (-2m_1/m_0^2)1/m_0]^T \tag{C.3}$$

rms duration, D

$$\mathbf{p}_D = \frac{\mathbf{p}_{D^2}}{2D} \tag{C.4}$$

Skewness cubed, S_t^3

$$\mathbf{p}_{S_t^3} = \begin{bmatrix} -\dfrac{m_3}{m_0^2} + 6\dfrac{m_2 m_1}{m_0^3} - 6\dfrac{m_1^3}{m_0^4} \\ -3\dfrac{m_2}{m_0^2} + 6\dfrac{m_1^2}{m_0^3} \\ -3\dfrac{m_1}{m_0^2} \\ \dfrac{1}{m_0} \end{bmatrix} \tag{C.5}$$

Skewness, S_t

$$\mathbf{p}_{S_t} = \frac{\mathbf{p}_{S_t^3}}{3S_t^2} \tag{C.6}$$

Normalized skewness, S

$$\mathbf{p}_S = \frac{\mathbf{p}_{S_t^3}}{3S_t^2 D} - \frac{S_t}{2D^3}\begin{bmatrix} \mathbf{p}_{D^2} \\ 0 \end{bmatrix} \tag{C.7}$$

Kurtosis to the fourth power, K_t^4

$$\mathbf{p}_{K_t^4} = \begin{bmatrix} -m_4 m_0^{-2} + 8m_3 m_1 m_0^{-3} - 18m_2 m_1^2 m_0^{-4} + 12m_1^4 m_0^{-5} \\ -4m_3 m_0^{-2} + 12m_2 m_1 m_0^{-3} - 12m_1^3 m_0^{-4} \\ 6m_1^2 m_0^{-3} \\ -4m_1 m_0^{-2} \\ m_0^{-1} \end{bmatrix} \tag{C.8}$$

Kurtosis, K_t

$$\mathbf{p}_{K_t} = \frac{\mathbf{p}_{K_t^4}}{4K_t^3} \tag{C.9}$$

Normalized kurtosis, $K = K_t/D$

$$\mathbf{p}_K = \frac{\mathbf{p}_{K_t^4}}{4K_t^3} - \frac{K_t}{2D^3}\begin{bmatrix} \mathbf{p}_{D^2} \\ 0 \\ 0 \end{bmatrix} \tag{C.10}$$

Root energy amplitude, A_e

$$\mathbf{p}_{A_e} = \frac{1}{2\sqrt{ED}}\left[\begin{bmatrix} 1 \\ 0 \\ 0 \end{bmatrix} - \frac{E}{2D^2}[\mathbf{p}_{D^2}]\right] \tag{C.11}$$